ICARUS **124,** 414–428 (1996)
ARTICLE NO. 0219

The Perseid Meteoroid Stream: Characterization of Recent Activity from Visual Observations

P. BROWN

Department of Physics, University of Western Ontario, London, Ontario, N6A 3K7, Canada; and International Meteor Organization, PF 600118, D-14401 Potsdam, Germany
E-mail: peter@danlon.physics.uwo.ca

AND

J. RENDTEL

International Meteor Organization, PF 600118, D-14401 Potsdam, Germany

Received February 27, 1996; revised June 26, 1996

The flux profile of the Perseid stream from 1988 to 1994 is analyzed using visual observations of meteors. The position and peak flux of recently detected outburst maxima are found for each year, as are the location and magnitude of the regular maximum. Details of the reduction procedure for these visual data are also presented. The Perseid stream is found to consist of three primary components: a long-lived and relatively weak background component, a core component which is active for 1–2 days near the main peak of the shower, and an outburst component which is active for only a few hours. The latter component changes position and strength dramatically from year to year, while the core maximum remains at a near constant location of $\lambda_\odot$ = 139°.96 ± 0°.05 and shows a variance of less than 30% from a mean peak flux of $S_{6.5\ \max}$ = 96 ± 16 meteoroids per 10^9 km^3 during 1988–1994. The outburst peak locations show no systematic variation from year to year, though the magnitude of the peak flux shows a significant difference for returns before 1991 compared to those after 1991. This may indicate an ejection origin other than 1862 for outburst material encountered before 1991. The particle composition of the outburst maximum and that of the core maximum are indistinguishable. A double maximum in the population index associated with these activity maxima has been detected in the average Perseid profile. High temporal resolution study of the flux profile of the ascending branches of the outburst profiles in 1993 and 1994 suggests that this component may consist of sub-components of differing ages. The mean visual flux of the shower is in excellent agreement with past radar results. The most important features of the stream gleaned from this study which must be explained by any model of the Perseids are also summarized.

1. INTRODUCTION

The Perseid meteor shower, recurring each year near August 12, is among the strongest and best known meteor showers currently visible on Earth. The prolific activity of the shower coupled with its occurrence during summer in the northern hemisphere has made it among the best known and best watched of astronomical events. According to Hasegawa (1993), the Perseids may have been chronicled for almost two milennia, making it among the oldest of the recorded showers. It was during the Perseid returns of the 1860s that the first crude orbit determination of the stream was made by Schiaparelli (1867), who found the stream to be in an orbit similar to that of 109P/Swift–Tuttle (1862 III). This was the first direct evidence connecting comets and meteor showers. A detailed historical review of the stream has been given by Kronk (1988).

Interest in the Perseids increased during the late 1970s in anticipation of the return of 109P/Swift–Tuttle, which was expected to reach perihelion circa 1980 (Marsden 1973). The comet, however, was not recovered within this time period. In 1988 and 1989 a new peak located some 12 hr before the regular Perseid maximum and of strength similar to the regular maximum was detected (Roggemans 1989, Koschack and Roggemans 1991). This new peak represented early detection of new meteoroids associated with the impending return of 109P/Swift–Tuttle. The position of the new activity peak in these years was very close to the nodal longitude of the comet ultimately recovered in September 1992 at $\lambda_\odot$ = 139°.44 (J2000.0) (Marsden *et al.* 1993, Yau *et al.* 1994). Subsequently, much stronger outbursts in activity were recorded from the Perseids between 1991 and 1994.

0019-1035/96 $18.00

Here we present a complete analysis of the detailed visual activity of the Perseid meteor shower near its time of maximum for the years 1988–1994. In total 14,552 count intervals were used for this study. This represents data collected by 1115 observers from 38 countries who reported 243,227 Perseid meteors during 14,237 hr of effective observational time. From these data we selected subsets which met all our criteria for inclusion in this work (see Section 2); we summarize these in Table I. In Section 2 we discuss briefly the method of observing used for all data analyzed and the basic procedures followed in reducing the data, including selection criteria for the observations, computation of the population index, r, the Zenithal Hourly Rate, spatial number density, S, and associated errors. The results of the reductions for each year are presented and briefly described for the entire shower interval in Section 3. In Section 4 results for short time interval analyses for the 1993 and 1994 Perseids are presented and described. In Section 5 we discuss the results and relate the salient features within each year's Perseid return to models of Perseid evolution and compare these results to those obtained with other methods of observation. In Section 6 we present the primary conclusions of the 7-year study and summarize the major features of current Perseid returns.

2. COLLECTION OF OBSERVATIONS AND THEIR REDUCTION

2.1. Method of Observation and Computation of the ZHR

The method used to observe meteors and reduce these data follows from the development of the visual techniques summarized by Kresáková (1966). Here we give an abbreviated discussion of the salient points and refer readers to more detailed discussions by Koschack and Hawkes (1995) and Koschack (1995). Of critical importance is the fact that these techniques are applicable to a single observer only; group observations where data are pooled cannot be used by this method.

In the most basic form, an individual observer using only the naked eye counts the number of meteors seen during a specified time interval and associates each with a certain shower or records it as a sporadic while also noting the magnitude of each meteor. During this time, the observer also notes the faintest star visible in his/her field of view (denoted the limiting magnitude (LM)) and records the total effective time that the sky was actually monitored (T_{eff}). The limiting magnitude of the portion of the sky monitored by the observer is determined by counting the number of stars visible in certain selected regions of the sky. The LM is usually the result of a weighted mean of several such measurements taken during the observation at intervals as determined by changing sky conditions and reported as averages to 0.01 M_v.

In what follows we describe briefly reduction techniques developed for visual observations. The interested reader is referred to other sources for more detailed discussions (cf. Koschack and Rendtel 1988, Koschack and Rendtel 1990a,b).

From each observation interval a quantity called the Zenithal Hourly Rate (ZHR) is calculated. The ZHR is the number of meteors from the shower a standard observer would see under unobstructed skies with the radiant point overhead and the LM = 6.5. This definition forms the basis for "standardization"; the goal of all reductions is to correct an imperfect observation to this standard. The ZHR is defined as

$$\text{ZHR} = \frac{N\, r^{6.5-\text{lm}}}{\sin^{\gamma}(H_{\text{rad}})\, T_{\text{eff}}}. \tag{1}$$

Here N is the number of shower meteors observed during the effective observing time T_{eff} with the radiant altitude being H_{rad} at the middle of the interval. An exponent $\gamma > 1$ has been proposed (Zvolánková 1983, Bellot 1995) as a proper correction, particularly for low radiant altitudes. For visual observations it has been shown that $\gamma \approx 1$ (Bellot 1995, Koschack 1994). Since we do not use observations for which the radiant is less than 20° altitude, we choose $\gamma = 1$ and do not risk serious error even if this is not strictly the case. The value r is the population index, defined as

$$r = \frac{N(M_v + 1)}{N(M_v)}, \tag{2}$$

where $N(M_v)$ is the total number of meteors of magnitude M_v or less. The population index characterizes the slope of the cumulative number vs magnitude for the shower and can be related to the differential mass index s with appropriate connection between mass and magnitude via (McKinley 1961)

$$s = 1 + 2.5 \log(r). \tag{3}$$

It is clear from (1) that the ZHR is a sensitive function of the background sky brightness and transparency—this results naturally from the power-law distribution in the number vs magnitude for meteors.

The selection criteria applied to all data in this study included a check to ensure that the Perseid radiant was above the horizon and at an altitude of at least 20° during the period activity from the shower was reported. As well, only those observations for which the total correction factor (the value multiplying N in Eq. (1)) was less than 5

and observations for which LM > 5.5 (with the exception of Perseid returns where the moon was present) were used. The individual ZHRs are then averaged over time intervals and systematic deviations from the average by each observer are used to establish an equivalent average perception. Once this value is known, the perception correction is applied to the observations through a change in the reported LM values (Koschack and Rendtel 1990b). In this way, the observing conditions are changed to precisely offset any differences in perception. The ZHR curve is then recalculated using these perception coefficients for each observer. While other methods for determining perception within a group of observers exist (cf. Öpik 1922), the method we employ provides accurate perception values for sufficiently large data sets without need for observers to be at the same location.

A final ZHR curve is computed based on a sliding average over short time intervals whose minimum size depends on the duration of the individual counting intervals. The interval length must always contain a statistically significant number of meteors. Close to the maximum an interval typically contains no less than 20 shower meteors. Generally, it is possible to achieve a temporal resolution of about half the size of the sampling interval for a given set of individual observations (all with the same counting interval). The final ZHR curve is then calculated after application of an algorithm to identify and reject individual ZHR values which deviate by more than 1.65σ from the mean in any interval.

2.2. The Population Index (r)

To determine accurate ZHRs, precise values of r as a function of solar longitude must be determined; knowing both of these quantities for a stream characterizes the shower completely. For a single observer, the value of r for a given night's observation for a specific shower is calculated by performing a least-squares fit to the magnitude vs cumulative number distribution reported for that shower. Each observer records meteors over a field of about 50° radius only (Koschack and Rendtel 1990a), with this effective field of view decreasing for fainter meteors. The perception probabilities for a given meteor magnitude depend on the difference in brightness between the meteor magnitude M_v and the limiting magnitude (LM) as well as on the angular distance between the observer's field center and the location of the meteor. By taking an average value for the perception over the entire field, one can find a probability of perception as a function of the magnitude difference $\mathrm{LM} - M_v$. By taking these perception probabilities in conjunction with the magnitude distribution for the shower, we can find the true number of shower meteors in each magnitude class appearing over the full 100° observer field of view via

$$N_{\mathrm{true}} = \frac{N_{\mathrm{obs}}}{p(\mathrm{LM} - M_v)}, \tag{4}$$

where N_{true} is the actual number of meteors which occurred over this region, N_{obs} is the number observed, and $p(\mathrm{LM} - M_v)$ is the probability of detection for a given sky limiting magnitude (LM) and meteor brightness (M_v). For faint meteors, the detection probability differs from observer to observer, while for the brighter meteors the differences in perception between observers become small. The detection probabilities determined for experienced observers have been used in this work. Here we consider only meteor magnitude classes with $(\mathrm{LM} - M_v) > 2$ and hence avoid the major source of error (the faint meteors which are most affected by different detection probabilities between observers) in the computation of r.

Once the true number of meteors appearing over the effective field of view is known for each magnitude class, a distribution of true cumulative number of meteors vs magnitude can be constructed. From (2), we expect the magnitude–number relationship for meteors to follow a power law and as a result we perform a least-squares fit on the magnitude–number relation in the form

$$\log_{10}(N_{\mathrm{cumtrue}}(M_v)) = M_v \log_{10}(r) + \log_{10} K, \tag{5}$$

where $N_{\mathrm{cumtrue}}(M_v)$ is the true cumulative number of meteors brighter than M_v, r is the population index, and K is a constant multiplier equal to the true number of meteors observed over the 100° field of view brighter than 0th magnitude.

This technique provides a measure for r valid over the length of time of the observation, usually an entire night (unless activity is very high). Each magnitude class must have a significant number of observed meteors (at least 3) and the two magnitude classes nearest the LM are excluded as previously described. As well, a minimum of five magnitude bins are required for any valid distribution, as are a total of at least 30 meteors within the entire sample. The magnitude distributions for individual observers satisfying these criteria are first found and individual r values determined for these observations. Then all remaining magnitude distributions from various observers are pooled to meet these criteria and used to compute additional values for r. These individual r values are then used to compute the final r profile in the same manner as the sliding-mean procedure for the ZHR profile.

2.3. Calculation of the Spatial Number Density

With the r profile and ZHR profile computed, the spatial number density in the stream can be determined. The only value missing in transforming to spatial number density

is the effective viewing area in the atmosphere for the visual observer.

In general, the collecting area in the atmosphere sampled by the visual observer at meteor heights (100 km) is dependent on the population index (due to effects of distance and extinction near the horizon which lessen a meteor's apparent magnitude) and the angular elevation at which the center of the observer's field of view is positioned. Fortunately, the collecting area in the atmosphere is significantly different only for extremely low elevations and is relatively unchanged over typical values for r ($2 < r < 3$) (Koschack and Rendtel 1990a). For an elevation of 50° and assuming the mean height of ablation to be 100 km, Koschack and Rendtel (1990a) derived the relation

$$A = 37{,}200\ \text{km}^2(r - 1.3)^{-0.748}, \tag{6}$$

where A is the effective collecting area in square kilometers. This effective collecting area is free of any significant atmospheric extinction due to angular elevation and has a distance to the observer of 100 km, implying that the measured magnitudes correspond to absolute meteor magnitudes.

To compute the spatial density one must correct the observed ZHR to a true ZHR accounting for those meteors missed in the observer's field of view. From these detection probabilities and a known value for r, the observed ZHR is corrected to the true ZHR. Thus we have that

$$\text{ZHR}_{\text{true}} = \text{ZHR}_{\text{observed}} C(r), \tag{7}$$

where ZHR_{true} is the true total number of meteors which occurred inside the observer's field of view and $C(r)$ is the conversion factor between the true and observed ZHR. From the standard perception probabilities, Koschack and Rendtel (1990b) determined $C(r)$ to be of the form

$$C(r) = 13.10r - 16.45. \tag{8}$$

Thus ZHR_{true} gives the total number of meteors of absolute magnitude +6.5 and brighter actually occurring over atmospheric area A in 1 hr of equivalent observing time if the radiant were at the zenith. Finally, the spatial number density can be found from

$$S = \frac{\text{ZHR}_{\text{true}}}{3600\,AV}, \tag{9}$$

where S is the number of meteoroids per km^3 which produce meteors of absolute magnitude 6.5 and brighter and V is the velocity of the meteoroid upon entry into the atmosphere in km/sec. The values for S are usually quoted in units of meteoroids per 10^9 km^3 for convenience.

2.4. Errors

For the ZHR, population index, and spatial number density profiles, the formal errors represent the standard deviations of the set of observations where all errors are taken to be uniformly random and the resulting distributions are assumed to be Gaussian. Generally, tens to hundreds of individual observations are available over any given observational interval, allowing meaningful determination of error within the context of statistical theory. These error values break down for small numbers of observations, but are generally applicable for the large data sets considered in this work. The effects of systematic errors are more difficult to establish, but data strongly affected in this way are detected through examination of secondary criteria (such as the sporadic rate) and removed from further analysis.

3. RESULTS OF PERSEID OBSERVATIONS 1988–1994

The ZHR activity, population index, and corresponding spatial number density profiles for the Perseid stream for each year from 1988 to 1994 are given in Figs. 1–7. Not shown in these figures are the sporadic hourly rates (HR) corrected for stellar limiting magnitude. These values are used during the initial selection cycle as indicators of systematic error in shower ZHRs. Since the observers contributing to the ZHR average at a given time are distributed over areas on the order of the size of a continent, the sporadic HR is not correctable in the same manner as the shower ZHR. This is a direct result of the fact that sporadic meteors do not have radiants distributed randomly over the celestial sphere (cf. Jones and Brown 1993), but rather are concentrated in several diffuse sources. This implies that the sporadic HR varies as a function of geographic latitude and local time in a non-trivial manner and thus cannot be used directly to correct relative shower rates from different locations.

Inspection of these curves shows that the level of flux appears to vary significantly throughout these years not only in the outburst component of the profile, but in the primary maximum as well. Some of this variation is due to lunar conditions as in 1990 and 1992. The corresponding profiles are uncertain as a result, this being most evident in the large errors in the population index profiles in these years caused by low limiting magnitudes and thus small numbers of faint meteors. The number of Perseid meteors, the total effective observing time, and the number of contributing observers for each year are given in Table I. The profiles also differ due to poor observer coverage, particularly in the Pacific region, and result in gaps during several years.

In spite of these difficulties, the large data sets clearly show that the level of Perseid activity is variable from year to year. The shapes of the ZHR and spatial number density

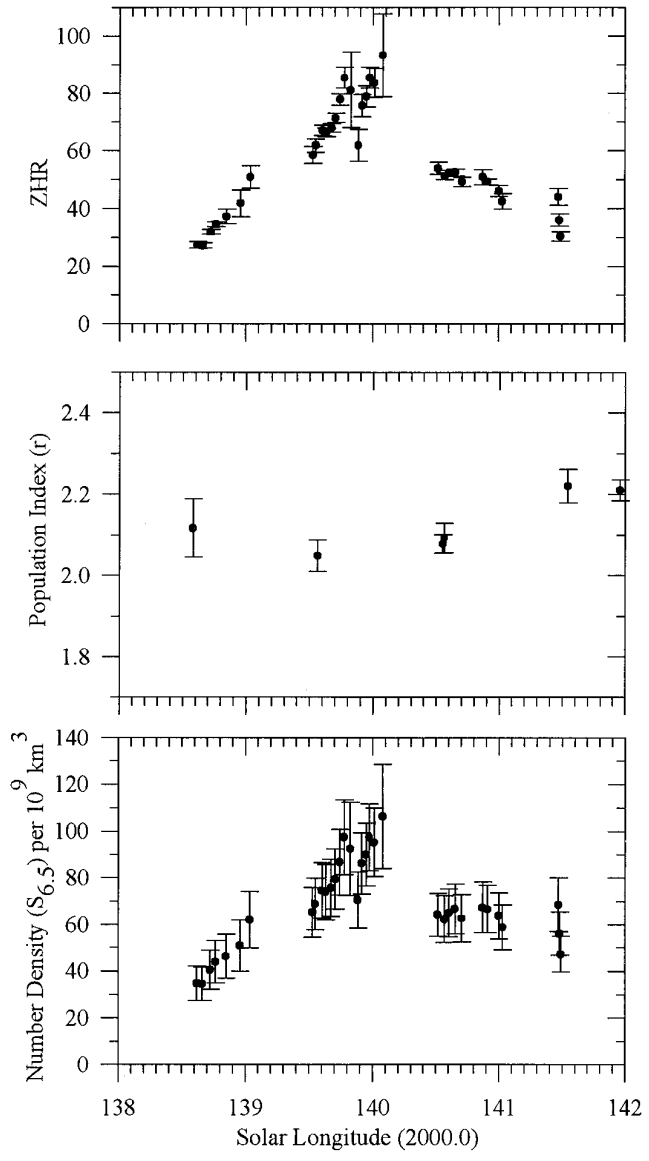

FIG. 1. The ZHR, r, and spatial number density ($S_{6.5}$) for the 1988 Perseid return.

profiles are generally similar, though significant variations in the population index, particularly after the main maximum, do tend to broaden the main peak in S. The spatial number density curves shown here are for a limiting absolute magnitude of 6.5 or equivalent limiting mass of 2×10^{-5} g, using the mass–magnitude–velocity correction of Verniani (1973). For the outburst portions of the profile, fainter meteors will tend to be under-represented as observers become overloaded recording shower meteors. This saturation effect has been documented in previous examinations of Perseid data (Koschack *et al.* 1993). The effect will be to make the S values smaller than the true values; hence the values shown here for the new peaks are lower limits.

In 1988, the data are well distributed about both maxima. This was the first year that the "new" maximum was detected, in this case at $\lambda_\odot = 139.^\circ78$, about 6 hr before the traditional peak, which took place at $\lambda_\odot = 140.^\circ08$ (Roggemans 1989). The old and new maxima were of very similar activity, but there are insufficient magnitude data to determine if the particle composition differed between the peaks. The ascending branch of the early maximum is well defined and shows a half-width-to-half-maximum (HWHM) activity above the general profile of 1 hr. The descending branch is not well defined, but the few data

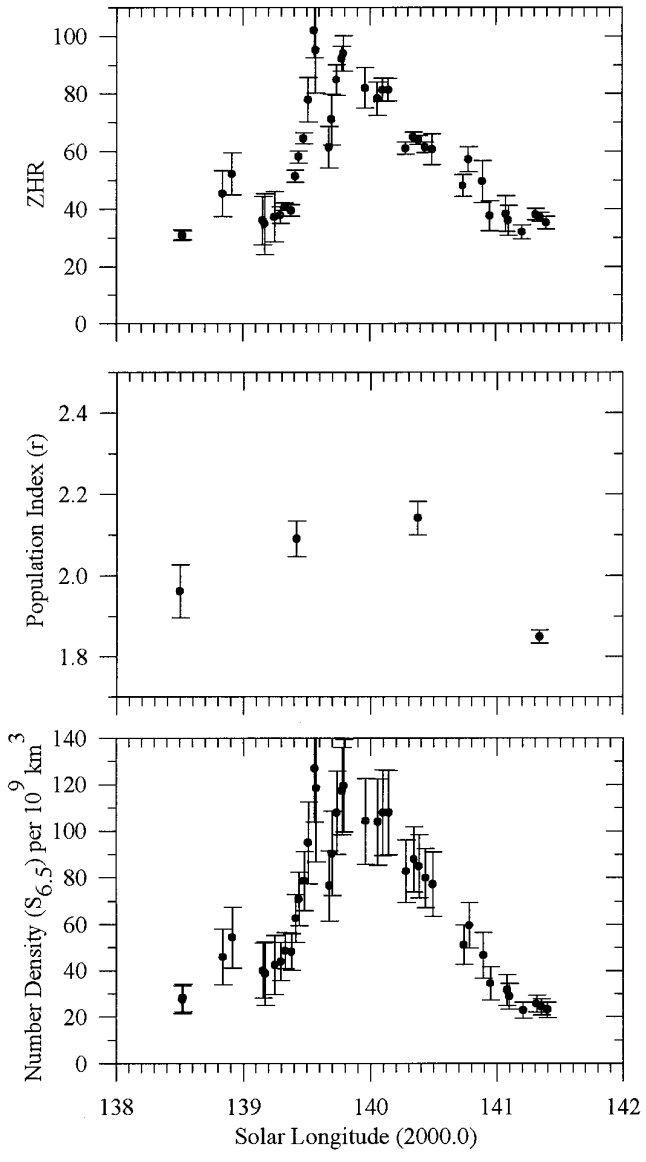

FIG. 2. The ZHR, r, and spatial number density ($S_{6.5}$) for the 1989 Perseid return.

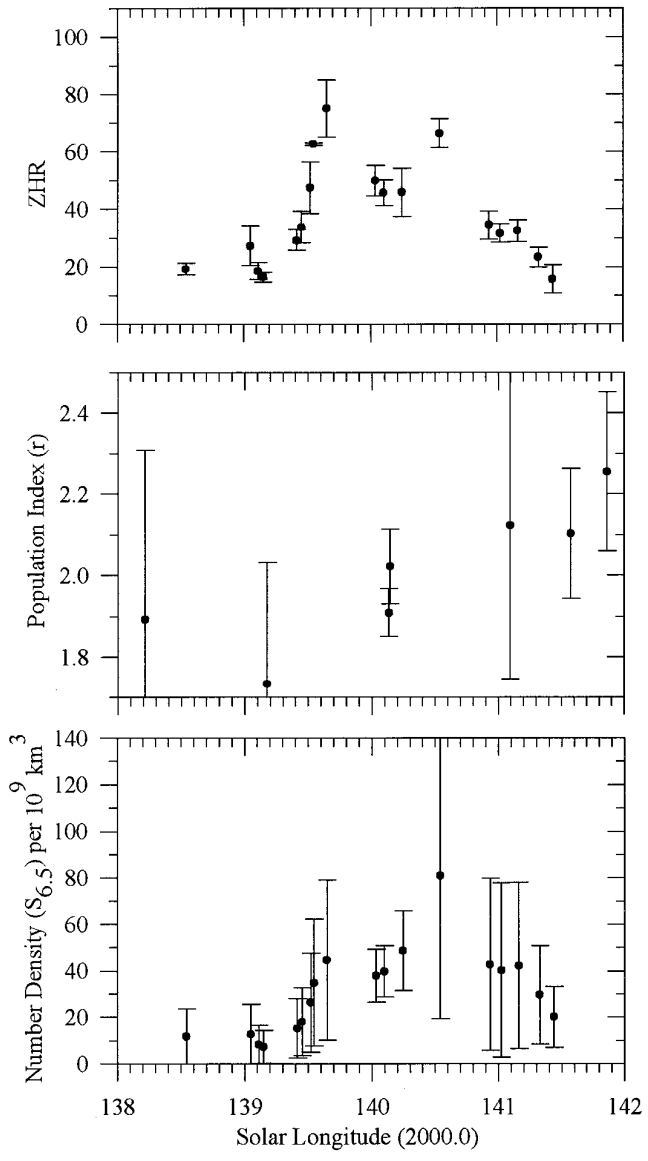

FIG. 3. The ZHR, r, and spatial number density ($S_{6.5}$) for the 1990 Perseid return.

here suggest a similar decline to a local minimum before activity again increases to the normal maximum. The descending branch of the main maximum is missing in these data and a higher maximum than shown here is possible, though the data do cover the interval during which the normal Perseid peak traditionally occurs and where it is well delineated in later data. The population index profile suggests a local dip of order a day in scale in the r value near the time of peak relative to the days before and after the maxima.

The 1989 profiles in Fig. 2 are similar to those for 1988 for times away from the maxima. The early maximum occurs at $\lambda_\odot = 139.^\circ56$ while the normal maximum is at $\lambda_\odot = 139.^\circ8$. The magnitudes of the maxima are again similar. The ascending branch of the early peak has a HWHM of 2 hr and is well defined. The descending branch from the early peak is absent in 1989 due to uneven observer coverage. The rising portion of the main profile shows a clear peak followed by several closely spaced points of decline, suggesting that the maximum is better located than in 1988. Several features are notable in the falling portion of the main maxima, namely at $\lambda_\odot = 140.^\circ1$ and $\lambda_\odot = 140.^\circ3$. The population index profile shows a broad minimum just before activity maximum.

Data for 1990 are heavily contaminated by the moon, which was full on August 6, 1990, and thus affected all

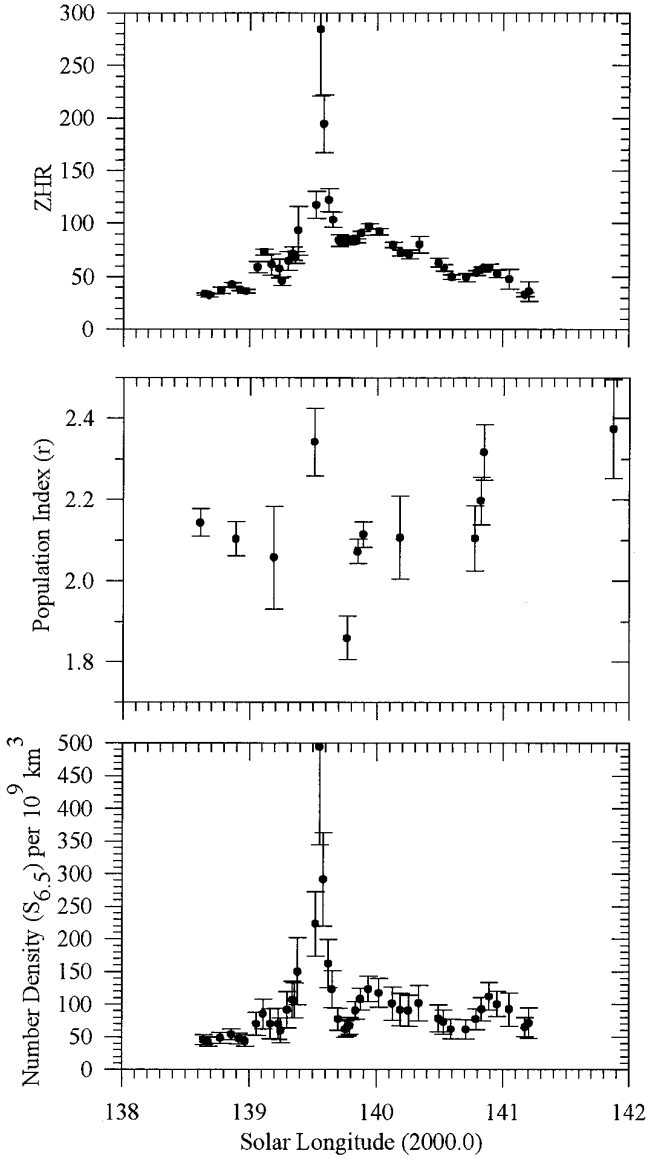

FIG. 4. The ZHR, r, and spatial number density ($S_{6.5}$) for the 1991 Perseid return.

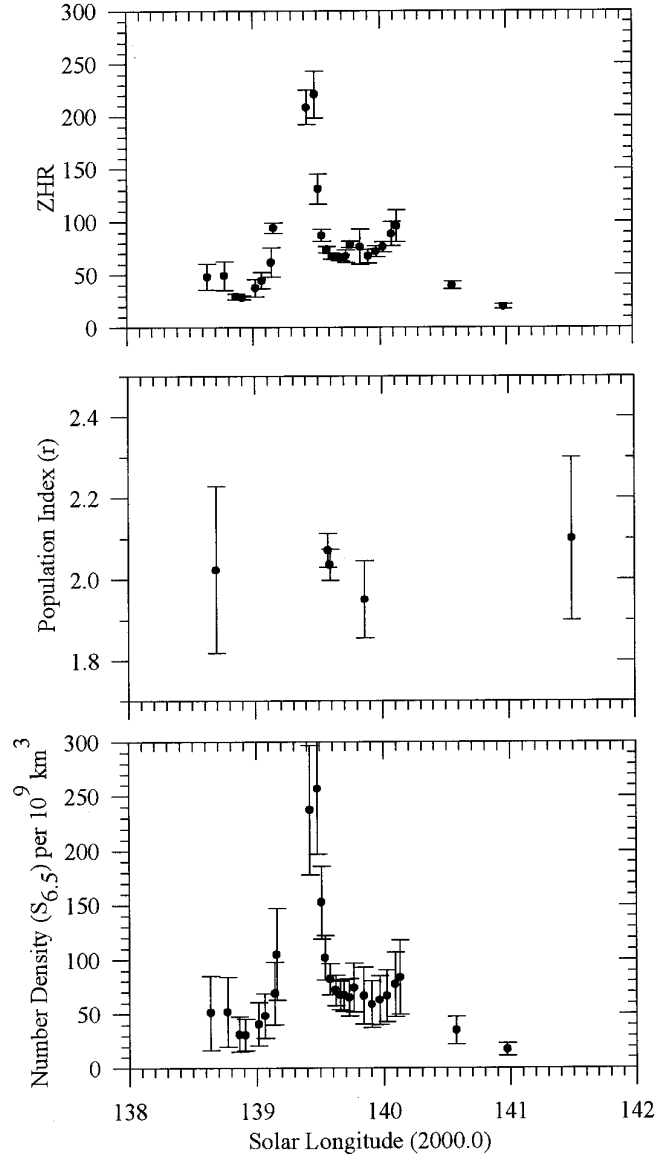

FIG. 5. The ZHR, r, and spatial number density ($S_{6.5}$) for the 1992 Perseid return.

observations during the peak. There appears to be a first peak near $\lambda_\odot = 139.^\circ6$ with a maximum ZHR value of roughly 75, with the later peak occurring near $\lambda_\odot = 140.^\circ5$ with a ZHR value of 66. Neither peak is defined by more than one or two low-weight data points. The extremely low ZHR values at peak are likely artifacts of the lunar conditions. Additional error is apparent from the shape of the sporadic activity curve, which closely mimics the Perseid curve, suggestive of numerous Perseids being counted as sporadic.

In 1991, the relative magnitudes of the two peaks become quite different, with the early peak becoming dominant. The peak times for the maxima are clearly resolved as $\lambda_\odot = 139.^\circ55$ and $\lambda_\odot = 139.^\circ94$, respectively. The ascending branch of the early peak has few data, but the HWHM can be roughly estimated as 0.5 hr. The descending portions have good coverage and reveal a HWHM of only 1 hr. The normal peak shows good coverage in 1991, displaying a HWHM value of 12 hr for the descending branch; the ascending branch value is uncertain due to contamination from the earlier peak. Additional activity features after the main maximum are prominent in this profile occurring at $\lambda_\odot = 140.^\circ34$, $140.^\circ9$. There is also an apparent difference in particle makeup across the broader profile, with a local minimum for r between the early and the main maximum.

The lunar conditions were poor in 1992 at the peak, with

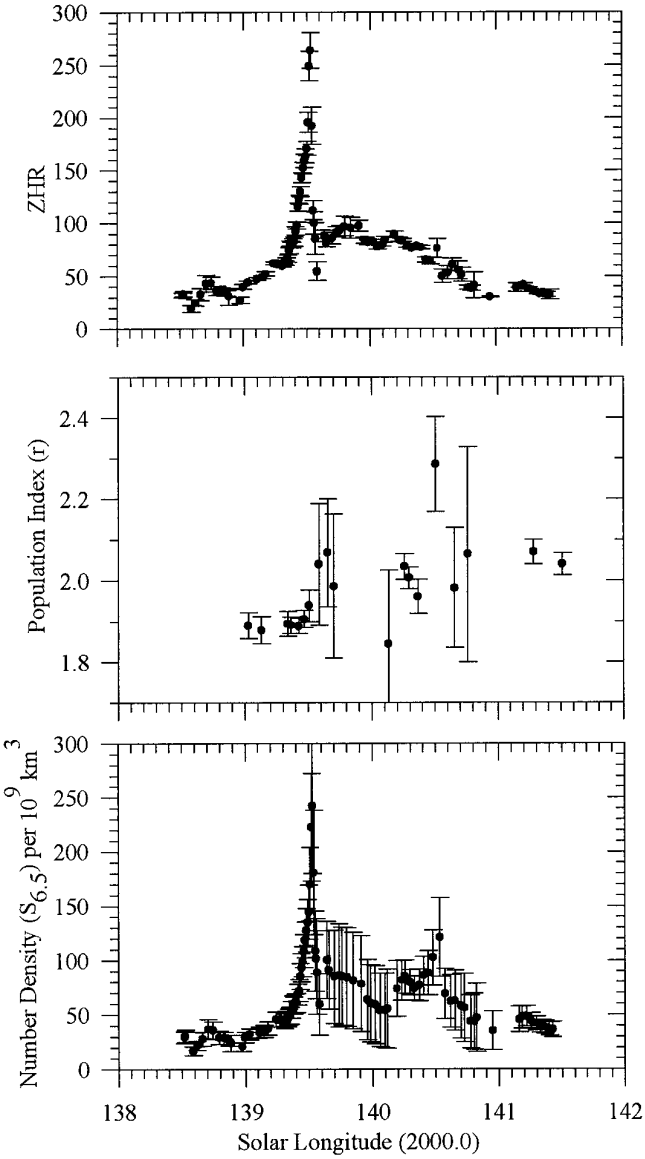

FIG. 6. The ZHR, r, and spatial number density ($S_{6.5}$) for the 1993 Perseid return.

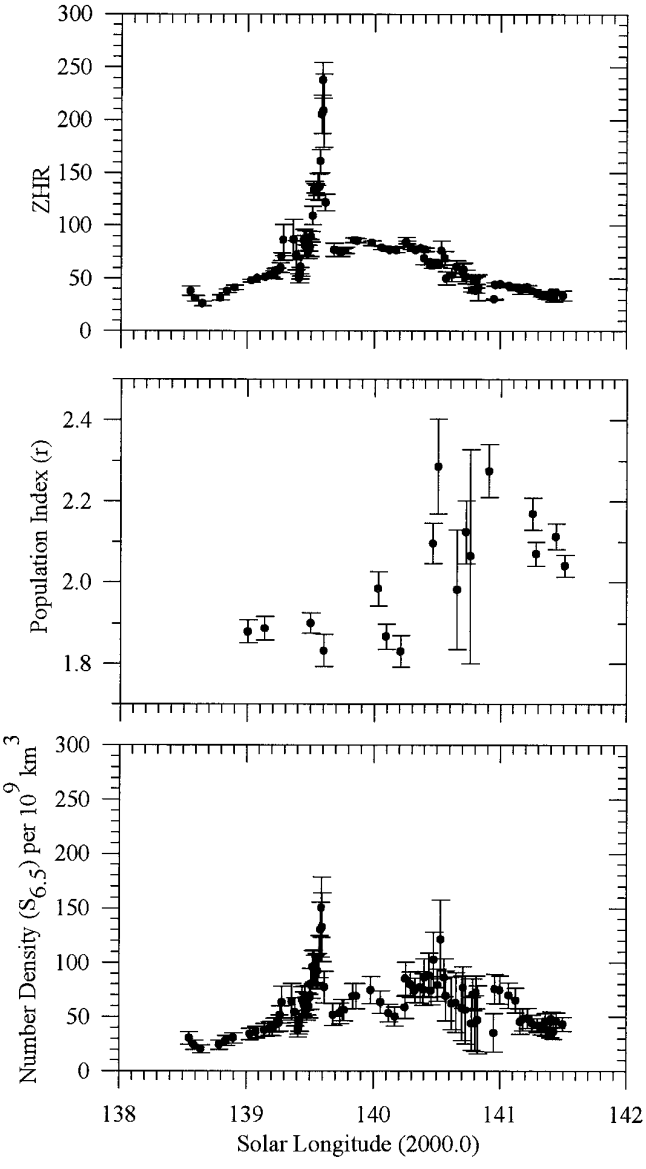

FIG. 7. The ZHR, r, and spatial number density ($S_{6.5}$) for the 1994 Perseid return.

full moon occurring on August 13. Nevertheless, good data coverage enabled better determination of the time of peak and its magnitude than in 1990. Information is obtainable about the descending portion of the early peak, which was approximately 1 hr HWHM and occurred at $\lambda_\odot = 139\overset{\circ}{.}48$. The main maximum appears at approximately $\lambda_\odot = 140\overset{\circ}{.}13$ with a ZHR of 90.

The 1993 shower had the best coverage of all years. The profiles in the ascending branch of the early peak are the clearest of any of the profiles, displaying a HWHM of 1.5 hr. The descending branch is not well delineated, but the data do suggest that the HWHM for the ascending branch was almost twice as wide as that for the descending branch,

TABLE I

The Number of Perseid Meteors, the Total Effective Observing Time, and the Number of Contributing Observers for Each Year of the Study

Year	Number of Perseids	Total observing time (hr)	Number of observers
1988	25,526 (38,037)	1033 (2571)	194 (230)
1989	16,708 (25,227)	647 (1930)	187 (261)
1990	1,547 (3,877)	115 (863)	46 (137)
1991	36,073 (44,762)	1045 (2079)	219 (262)
1992	6,462 (10,870)	326 (1290)	105 (195)
1993	59,080 (81,538)	1768 (3211)	409 (454)
1994	33,210 (47,165)	1041 (2428)	268 (347)
1988–1994	206,872 (251,476)	13,538 (14,372)	1089

Note. The numbers in parentheses represent the raw data and the 1988–1994 column represents the values for the reference profile. The latter are not simple sums of the previous rows due to exclusion of the time periods containing the outburst peak in the reference profile.

with the early peak occurring at $\lambda_\odot = 139\overset{\circ}{.}53$. The main ZHR maximum was broad in extent, occurring near $\lambda_\odot = 139\overset{\circ}{.}9$. A prominent secondary peak after the main maximum in both the ZHR and spatial number density profiles is located at $\lambda_\odot = 140\overset{\circ}{.}2$. The spatial number density profile also suggests that a secondary maximum in the flux occurred at $\lambda_\odot = 140\overset{\circ}{.}5$ accompanying a large increase in r. There is a clear dip in the r profile at the time of the early peak, but this may be due to saturation effects.

In 1994 good observer coverage and excellent lunar conditions converged. The ascending portion of the profile is well established, with the early maximum occurring at $\lambda_\odot = 139\overset{\circ}{.}59$ and displaying a HWHM of only 1 hr. The magnitude data are particularly well defined in 1994 and show a decrease in r after the early peak. A strong asymmetry is present in the population index before and during maximum compared to after both peaks, when its value becomes much larger. The main peak occurs near $\lambda_\odot = 139\overset{\circ}{.}9$, but is difficult to locate precisely due to its broad outline. There is another clear feature in the descending portion of the profile near $\lambda_\odot = 140\overset{\circ}{.}3$ as well as one at $\lambda_\odot = 140\overset{\circ}{.}5$.

These results are summarized in Table II.

4. HIGH TEMPORAL RESOLUTION SERIES

To determine if any structure is present in the outburst component of the stream, the data for 1993 and 1994 near the locations of the outburst have been re-analyzed at higher temporal resolutions. Small-scale variations in flux profiles near the time of outbursts have been reported in the past associated with the Draconids (Lovell 1954, p.

TABLE II
The Locations and Magnitude of the Perseid Maxima from 1988 to 1994

Year	$\lambda_{\odot 1}$	$ZHR_{outburst}$	$S_{6.5\ outburst}$	$\lambda_{\odot 2}$	ZHR_{max}	$S_{6.5\ max}$
1988	139°.78 ± 0°.03	86 ± 4	97 ± 16	140°.08 ± 0°.04	106 ± 22	94 ± 14
1989	139°.56 ± 0°.03	102 ± 10	127 ± 23	139°.80 ± 0°.09	94 ± 6	120 ± 20
1990	139°.55 ± 0°.05	75 ± 10	45 ± 35	140°.54 ± 0°.2	81 ± 61	66 ± 5
1991	139°.55 ± 0°.03	284 ± 63	494 ± 150	139°.94 ± 0°.04	97 ± 2	124 ± 20
1992	139°.48 ± 0°.02	220 ± 22	257 ± 60	140°.13 ± 0°.2	84 ± 34	96 ± 15
1993	139°.53 ± 0°.01	264 ± 17	242 ± 62	139°.91 ± 0°.04	86 ± 2	79 ± 44
1994	139°.59 ± 0°.01	238 ± 17	151 ± 28	139°.84 ± 0°.04	86 ± 2	69 ± 12
1988–1994	—	—	—	139°.96 ± 0°.05	86 ± 1	96 ± 16

Note. $\lambda_{\odot 1}$ is the position of the first (new) maximum and $\lambda_{\odot 2}$ is the position of the second or normal maximum. The spatial number densities associated with the first peak ($S_{6.5\ outburst}$) and the second or normal maximum ($S_{6.5\ max}$) are also given in units of meteoroids brighter than absolute magnitude +6.5 per 10^9 km^3.

330) and α-Monocerotids (Rendtel *et al.* 1996). Here all count intervals greater than 0.5 hr were rejected to obtain a high resolution profile with steps as short as 0°.004 in the solar longitude in the immediate region near the outburst peak. Strictly speaking, these averaging intervals are too short if they consist predominately of 1/2 hr (or longer) counting intervals, but fortunately most count intervals in this period are of the order of 5–15 min duration. The results are shown in Figs. 8 and 9, where details of the averaging intervals and step lengths are given. Note that 1993 Perseid data are more than an order of magnitude more plentiful than those in 1994.

The buildup to maximum in 1993 is extremely well defined and shows two main components: a gradually increasing branch beginning at $\lambda_\odot$ = 139°.35 and continuing to $\lambda_\odot$ = 139°.49. In this interval, the slope of the spatial number density—solar longitude curve—is +7.5 meteoroids per 0°.01 of solar longitude brighter than +6.5 (hereafter $(M_v > 6.5)\ 0°.01^{-1}$). In the interval from 139°.49 to 139°.53 the slope changes dramatically to +43 $(M_v > 6.5)\ 0°.01^{-1}$. These two sections suggest that the outburst component may itself consist of several sub-components of differing ages, the steep increase being associated with the most recent ejecta and the broader increase just before it due to material diffused somewhat from slightly older passages of Swift–Tuttle. Since the nodal longitude of Swift–Tuttle has been gradually increasing over time, one expects the oldest ejecta to be preferentially before the current nodal longitude of the comet.

This effect is further reflected in the descending component of the profile. Though less defined it shows a steep decrease, having a mean slope of −102 $(M_v > 6.5)\ 0°.01^{-1}$ in the interval 139°.53–139°.55.

The profiles in both the ascending and descending portions of the outburst in 1993 are remarkably smooth. Only hints of slight variations near 139°.45 and 139°.39 are present. Similar structure is also visible in the 1994 profiles near 139°.43 and 139°.51. Of interest is to note that the first of these is in a location similar to that of the structure present in 1993 and that these are both extremely close to the current nodal longitude of 109P/Swift–Tuttle. The latter

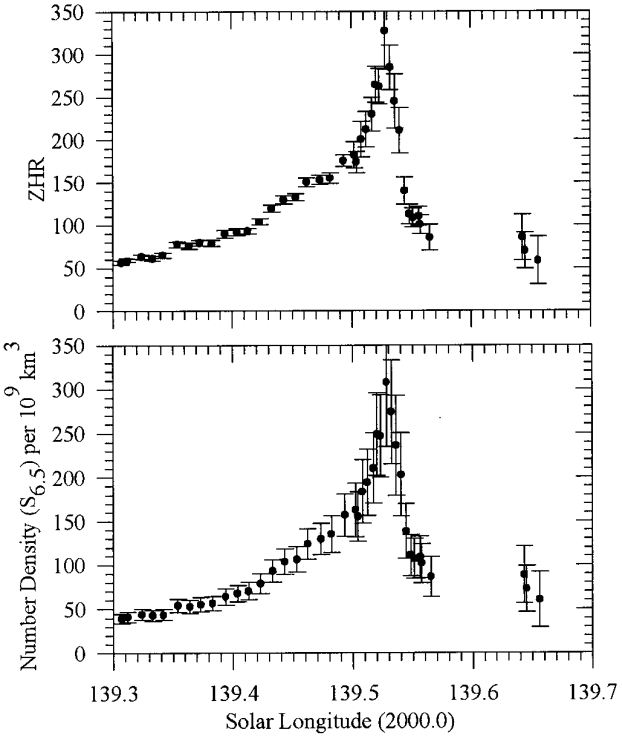

FIG. 8. The ZHR and spatial number density ($S_{6.5}$) for the 1993 Perseid return using higher temporal resolution. In total 1260 individual count intervals were available that were shorter than 0.3 hr in length during the central interval and 0.6 hr duration in the outer intervals. Between $\lambda_\odot$ = 139°.30 and 139°.50 the sampling interval was 0°.02 in length and shifted by 0°.01. From 139°.50 to 139°.56 the sampling interval was 0°.008 in length and was shifted by 0°.004. From 139°.56 to 139°.70 the sampling interval was 0°.02 in length, shifted by 0°.01.

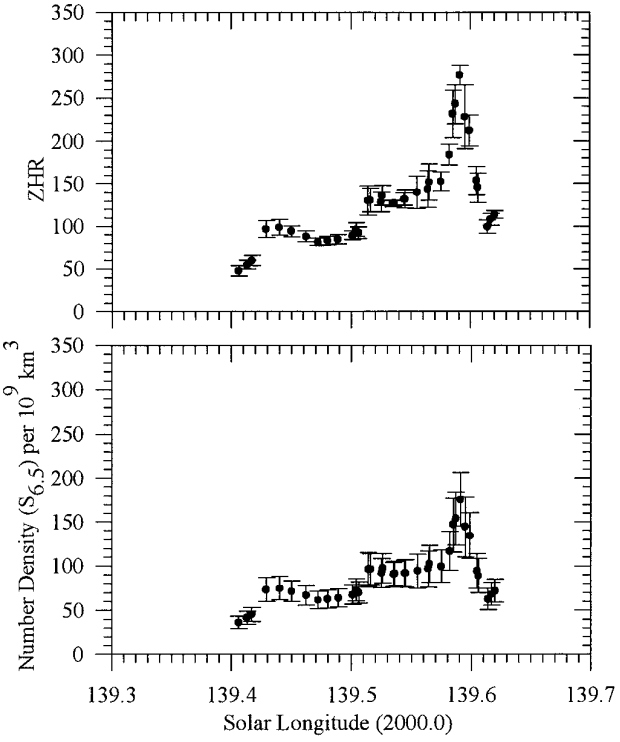

FIG. 9. The ZHR and spatial number density ($S_{6.5}$) for the 1994 Perseid return using higher temporal resolution. In total 124 individual count intervals were available that were shorter than 0.3 hr in length during the central interval and 0.5 hr duration in the outer intervals. Between $\lambda_\odot$ = 139°.30 and 139°.50 the sampling interval was 0°.02 in length and shifted by 0°.01. From 139°.50 to 139°.62 the sampling interval was 0°.008 in length and was shifted by 0°.004. From 139°.62 to 139°.70 the sampling interval was 0°.02 in length, shifted by 0°.01.

fluctuation in 1994 corresponds closely to the location of maximum in 1993 and suggests that many of the meteoroids associated with the outburst maxima have a small spread in semi-major axis amounting to only a few tenths of an AU or are perturbed into Earth-intersecting orbits effectively for intervals of order 1 yr.

In 1994, the outburst profile has fewer data and is less well defined. The buildup to the outburst peak is much slower than that in 1993, showing a plateau in activity with a "jump" in activity near 139°.51. The slope of the steeper rising ascending section of the outburst from 139°.57 to 139°.59 is 50 ($M_v > 6.5$) 0°.01^{-1}, very similar to the slope found in 1993. The descending branch of the profile has a slope of −53 ($M_v > 6.5$) 0°.01^{-1} from 139°.59 to 139°.61, which is significantly less than that in 1993, though the descending portion of both profiles are not well covered.

5. DISCUSSION

The Perseid stream as described from the visual observations presented here can be broadly partitioned into three major components: a broad plateau displaying weak activity (background Perseids), a more concentrated component centered about the traditional Perseid peak (core Perseids), and a strongly time-varying component of short duration which appears in all profiles shortly after the nodal longitude of the parent comet (outburst Perseids). To see more clearly the first two components, which have only modest variations from year to year, we have synthesized a mean Perseid curve from all available visual observations 1988–1994, but excluding those intervals obviously dominated by the outburst component. The ZHR profile for this average curve, the associated sporadic rate, and the mean population index profile, along with the spatial number density profile for the stream, are shown in Fig. 10 over the entire period of activity. These same quantities are also shown for the 10-day interval centered about the main Perseid peak in Fig. 11.

The background component is long-lived and shows weak activity extending from late July (≈115°) until the end of August (≈150°). This portion of the Perseid stream shows a very gradual increase in activity until ≈138°, at which time the activity profile steepens as the core portion of the stream is encountered. The core component rises to a peak whose long-term position is $\lambda_\odot$ = 139°.96 ± 0°.05. The steepest section of the peak associated with the core Perseids is very symmetrical, the ascending portion having a HWHM of 1°.06 ± 0°.07 compared to the descending HWHM of 1°.04 ± 0°.07. The slight asymmetry in the overall shape of the ZHR curve is most evident at the 1/4-width points, located 2°.58 ± 0°.07 before maximum and 2°.35 ± 0°.07 after maximum. From these results, the Perseid shower is above the sporadic background from ≈136° to 143° or roughly 1 week.

That the average Perseid profile is a superposition of two components and is asymmetrical has been known for some time from visual observations (cf. Ahnert-Rohlfs 1952, Lindblad 1986, Mason and Sharp 1981, Zvolánková 1984) as well as from radar data (Šimek and McIntosh 1986, Lindblad and Šimek 1986, Šimek 1987). Harris *et al.* (1995) have modeled the overall activity of the stream through decay of 109P/Swift–Tuttle over a 160,000 year time period. Their model reproduces the asymmetry in the core portion of the stream and also predicts several strong secondary maxima before the main peak, most notably one lasting several days at $\lambda_\odot$ = 125°. Such secondary maxima are not present in the mean profile presented here. One explanation for this is that the role of planetary perturbations on stream meteoroids is significant over very long time scales, even for high inclination streams such as the Perseids; the Harris model ignored such perturbations.

Little structure is evident in the mean ZHR profile, with the possible exception of a maxima near $\lambda_\odot$ = 140°.9 and a slight maxima at $\lambda_\odot$ = 139°.5, the latter undoubtedly related to the outburst component of the stream which has

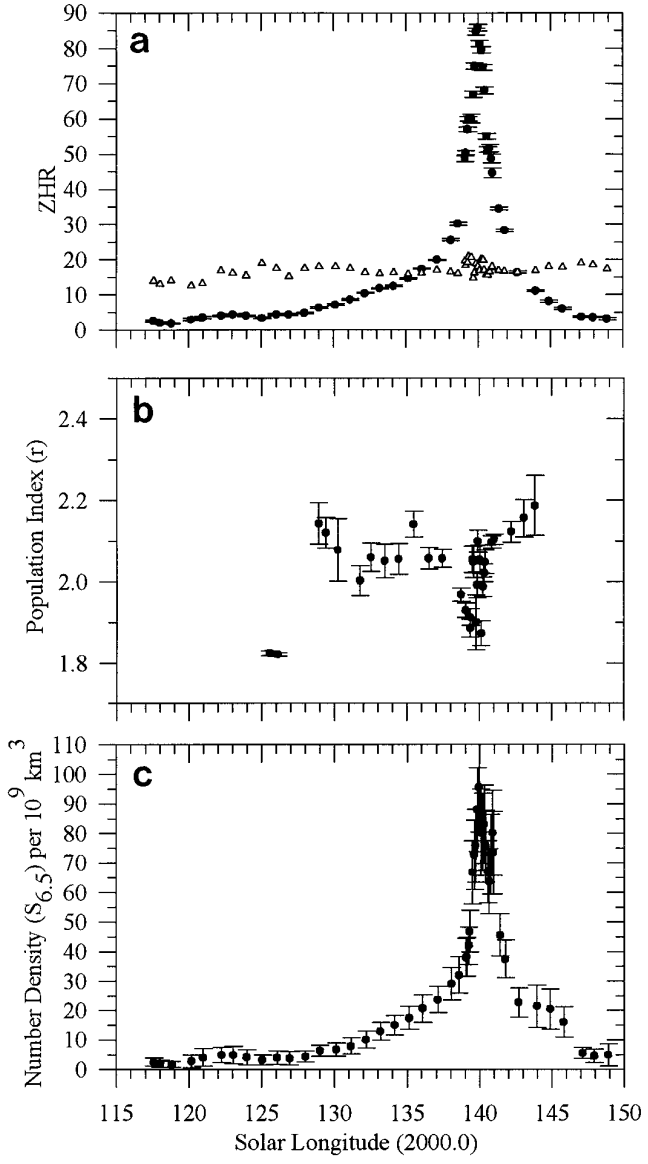

FIG. 10. The ZHR, r and spatial number density ($S_{6.5}$) for the mean Perseid activity (1988–1994) and the associated sporadic rate (HR) denoted by △ for the full duration of significant activity for the shower.

not been entirely filtered from these data. In addition to these local features, a broad plateau of flux is clearly visible in the spatial number density profile immediately following the main maximum. This is a consequence of the increase in r after the main maximum.

The lack of strong sub-maxima is an expected result, as the smoothing procedures tend to smear out any large variations in activity, such sub-maxima being visible primarily in the yearly profiles. Stable sub-maxima in long-term profiles have been noted previously, particularly in radar data on the stream. Table III summarizes the reported locations of past sub-maxima detailed in the literature as well as the main maximum. Possible sub-maxima active in specific years from this study are also given in the table. Previous visual and radar studies have suggested stable sub-maxima near $\lambda_\odot = 140\overset{\circ}{.}5$. There are indications of a sub-maximum in the 1993 and 1994 profiles near this position and it is worth noting that these years had far better coverage after the main maximum than any of the other years, but the most convincing candidates for sub-maxima in these years are located in the region $\lambda_\odot = 140\overset{\circ}{.}2–140\overset{\circ}{.}3$. That sub-maxima are present in some years appears probable given the high statistical weight of the visual reports in the present study, but stability of such

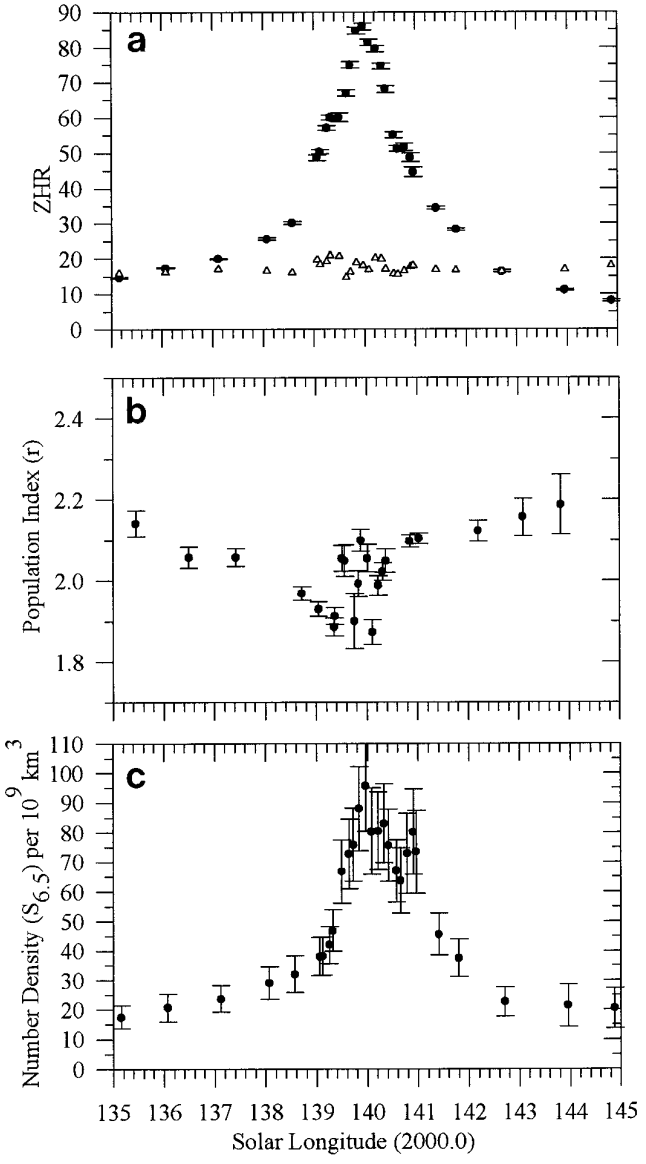

FIG. 11. The ZHR, r, and spatial number density ($S_{6.5}$) for the mean Perseid activity (1988–1994) and the associated sporadic rate (HR) denoted by △ for the 10-day interval centered about the activity peaks.

TABLE III
Locations of the Main Maximum and Reports of Sub-maxima from Recent Radar and Visual Data

Year(s)	$\lambda_\odot$	$\lambda_{\odot sub}$	Source
1980	139°.92 ± 0°.04		Mason and Sharp (1981)
1958–1962, 1972, 1980–1985	139°.89 ± 0°.035	139°.0, 139°.5, 140°.5, 142°.0	Šimek (1987)
1958–1964	139°.91 ± 0°.026	140°.5	Šimek and McIntosh (1986)
1953–1978	139°.90 ± 0°.035	140°.46	Lindblad and Šimek (1986)
1953–1981	140°.11	140°.45	Lindblad (1986)
1964–1981	139°.7 ± 0°.2		Andreev *et al.* (1987)
1989	139°.80 ± 0°.09	140°.1, 140°.3, (140°.9)	This work
1991	139°.94 ± 0°.04	(140°.34), 140°.9	This work
1993	139°.91 ± 0°.04	140°.2, (140°.5)	This work
1994	139°.84 ± 0°.04	140°.3, (140°.5)	This work

Note. $\lambda_\odot$ is the position of the main maximum and $\lambda_{\odot sub}$ is the position of any additional sub-maxima. Possible sub-maxima from this work are also given; those values which are less certain are shown in parentheses.

structures over many years is still questionable based on our results. Such structures may be linked with mean motion resonances operating in the Perseid stream as has been suggested by Wu and Williams (1995). Local maxima may simply be manifestations of groups of meteoroids with common ejection origin sharing similar values of nodal longitude and semi-major axis and thus being more numerous in one year than another. This sharp variation in the flux would be a direct result of a sharp peak in the distribution of semi-major axes within such a meteoroid sub-population.

In contrast, the main maximum shows a generally stable peak flux. Indeed, the peak spatial number densities from 1988 to 1994 associated with the main maximum vary from the average value $S_{6.5\,max}$ of 96 ± 16 by less than 30%. This result is in contradiction to past visual results which suggest large variations in $S_{6.5\,max}$. Zvolánková (1984) and Lindblad (1986) report variations by more than a factor of 2 in peak rates from visual observations made between the years 1944–1953 and 1953–1981, respectively. We suggest that these apparent variations are the result of biased sampling in these past visual observations resulting from uneven observer coverage.

The changes in $S_{6.5}$ associated with both maxima are given in Table II. The average values of $96 \pm 16 \times 10^9$ km^3 for $S_{6.5\,max}$ and $11 \pm 2 \times 10^9$ km^3 for $S_{3.5\,max}$ are in close agreement with the results of Kaiser *et al.* (1966) and Andreev *et al.* (1987), who, from radar observations, derive an average $S_{6.5\,max}$ of $1.3 \pm 0.2 \times 10^2 \times 10^9$ km^3 and an $S_{3.5\,max}$ of 14×10^9 km^3, respectively. Both radar observations were made at low frequency and thus should be relatively free of initial–train radius effects.

The variation in the population index of the stream shows several features (see Figs. 10b and 11b). The most apparent is the asymmetry in particle makeup in the day leading to the main maximum when r is consistently low compared to after the main maximum, when r shows a significant increase. The average value of r for the remainder of the profile, both before and after the maxima, is remarkably constant near 2.15. Two pronounced maxima in r are also evident near the time of the activity maxima. The first maxima in r occurs at $\lambda_\odot = 139°.55 \pm 0°.07$ and the second at $\lambda_\odot = 139°.88 \pm 0°.06$. That these features are statistically significant can be assessed from Table IV, where the number of Perseid meteor magnitude estimates used to derive each r value is given. These locations are potentially linked to the different evolutionary components of the stream. The first is probably related to the outburst component, which is still present despite removal of the central portions of the outburst activity in each year. The young meteoroidal material associated with the latest return of Swift–Tuttle is enriched in smaller meteoroids

TABLE IV
The Population Index, r, and the Number of Data that Each r Value Is Based upon for the Average Profile 1988–1994

$\lambda_\odot$	r	Number of observers	Number of perseids
139°.045	1.930 ± 0.018	172	11,931
139°.354	1.886 ± 0.022	101	10,257
139°.362	1.913 ± 0.021	118	11,369
139°.508	2.054 ± 0.032	43	2,806
139°.562	2.049 ± 0.039	27	1,870
139°.752	1.900 ± 0.068	13	1,140
139°.828	1.992 ± 0.032	70	9,001
139°.878	2.099 ± 0.027	83	11,641
140°.011	2.055 ± 0.034	61	5,664
140°.107	1.873 ± 0.031	76	5,389
140°.224	1.987 ± 0.024	117	9,660
140°.307	2.022 ± 0.022	162	15,257
140°.370	2.049 ± 0.029	96	9,638

Note. The solar longitude is the mid-point of the interval overwhich averaging occurred.

as would be expected for recent ejecta. The main maximum is also enriched in fainter meteors, indicating the presence of relatively young material.

A single local minimum in the population of small meteoroids just before maximum has been previously noted by Mason and Sharp (1981). Andreev *et al.* (1987) find a local maximum in the proportion of small meteoroids at the time of maximum from radar data. It seems probable that the different ages of the outburst and core components of the stream are manifest not only in higher flux but also in differences in the meteoroid population relative to the background population and that recent ejections of fresh meteoroids have significantly different r values as shown by these visual data.

The outburst component of the stream has been recognized in visual observations only over the last few years (cf. Roggemans 1989), though Lindblad and Porubčan (1994) have shown that photographic Perseid activity dating back as far as the 1950s had an earlier peak near the present nodal longitude for 109P/Swift–Tuttle. Šimek and Pecina (1996) also detected the presence of the outburst peak as early as 1986 in Ondřejov radar data and suggest that the sub-maxima reported at $\lambda_\odot = 139\overset{\circ}{.}5$ by Šimek (1987) in earlier radar data may also be a detection of the outburst component of the stream. This component has been widely associated with the return of 109P/Swift–Tuttle to perihelion in 1992 and is generally regarded as consisting of material only one or at most a few revolutions old (Wu and Williams 1993, Williams and Wu 1994, Jones and Brown 1996).

The positions of the outbursts given in Table II show no clear variation as a function of the year. The relative magnitudes of the peaks are shown in Fig. 12a, where the number densities at the outburst peak are given relative to $S_{6.5\ \mathrm{max}}$. Here a clear demarcation occurs, with activity being weak before 1991 and strong thereafter. This sudden change in the outburst component, rather than a gradual increase in flux as predicted by model calculations presuming all new activity to result from 1862 ejecta (Williams and Wu 1994), suggests that meteoroids encountered before 1991 may have a different origin. On the basis of model calculations, Jones and Brown (1996) ascribe the material from 1988–1990 almost exclusively to the 1737 and 1610 passages of Swift–Tuttle, with meteoroids from the 1862 passage first being encountered in significant quantities in 1991.

The location of the visual maxima in these years is very similar to that reported from overdense radar observations. Watanabe *et al.* (1992) analyzed the 1991 Perseid return with the Kyoto MU-radar and determined the time of peak for the outburst component to be $\lambda_\odot = 139\overset{\circ}{.}6$, in good agreement with the visual results. They also found that the outburst peak flux was 3.4 ± 0.8 times that of the main maximum. This result was valid for meteors in the magnitude range $0 > M_v > +3$, which is very similar to the ratio of spatial number densities we find between the outburst peak and the core maximum in 1991 of 3.2 in the same magnitude range. For comparison, Šimek and Pecina (1996) used the Ondřejov radar and found the maximum to be located at $\lambda_\odot = 139\overset{\circ}{.}58 \pm 0\overset{\circ}{.}04$ in the interval 1986–1994.

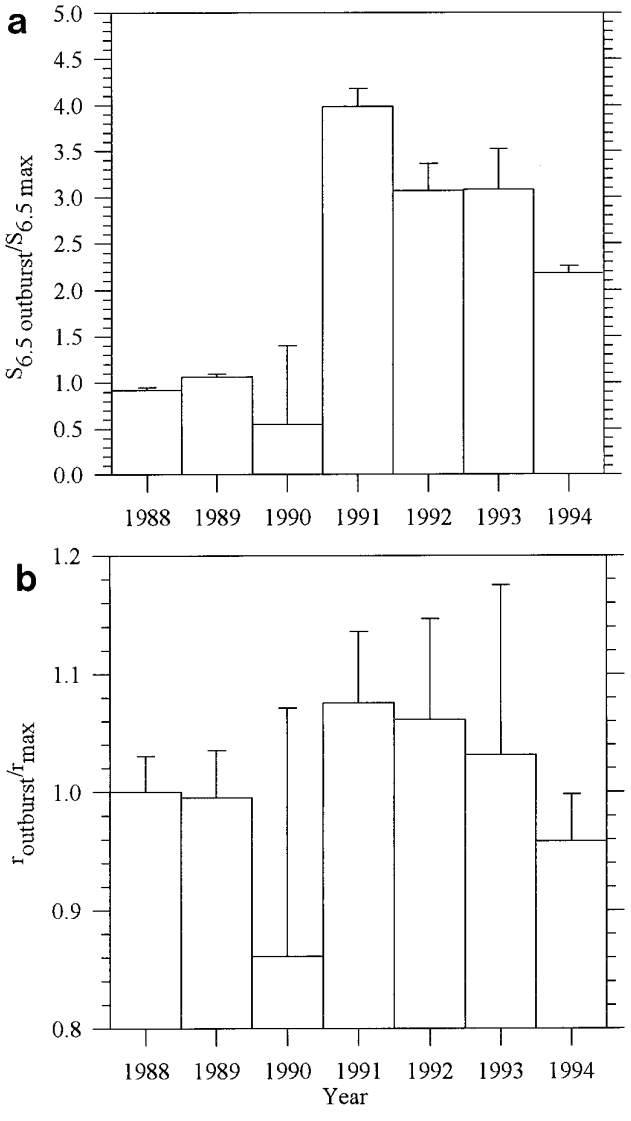

FIG. 12. The relative magnitude of the peak number density for the outburst component of the Perseids, $S_{6.5\ \mathrm{outburst}}$, in units of $S_{6.5\ \mathrm{max}}$ for the given year (a). The change in relative particle composition between the outburst peak and the main peak during 1988–1994 as denoted by the ratio of their respective population indices $r_{\mathrm{outburst}}/r_{\mathrm{max}}$ (b).

The particle composition of the outburst component of the stream is shown in Fig. 12b relative to the main peak, where the ratios of the respective population indices have been plotted. Watanabe *et al.* (1992) report an increase in the proportion of large meteoroids during the outburst

in 1991 and this notion has been variously supported by qualitative reports from observers during other Perseid outbursts (cf. Pin-xin 1992). There is little question that the number of bright Perseids increases during the outbursts. Figure 12b, however, shows that the proportion of bright meteors during the outbursts is not substantially different from the main peak and thus the mass distribution of the outburst in all years, as measured by r, is not different from the population associated with the core component of the stream, in contradiction to the conclusions of Watanabe *et al.* (1992). This result is consistent with the earlier observation of a maximum in the r values near the time of both maxima.

6. CONCLUSIONS

The 7-yr study of the Perseid stream presented here makes clear that visual meteor observations provide a useful diagnostic of stream activity. The correspondence between the radar data and the visual data shows the utility of both and the complementary nature of these two observational forms in meteor astronomy. The general validity of the reduction methods presented here for visual observations has been verified through early detection in 1988 of new material associated with the impending return of 109P/Swift–Tuttle (Roggemans 1989). This is the first time that visual meteor data have successfully ''detected'' the return of a comet through subtle variations in shower activity profiles before the comet was actually recovered.

From the flux data and particle population presented here for the Perseid stream, several outstanding features of the stream must be explained by any successful Perseid model:

1. The asymmetry in the background Perseids and the symmetry in the core population as defined by the locations of the 1/4-width(2°.58 ± 0°.07 before maximum and 2°.35 ± 0°.07 after maximum) and the 1/2-width (1°.06 ± 0°.07 before maximum and 1°.04 ± 0°.07 after maximum) positions.
2. The location and magnitude of the outburst maxima for each year given in Table II.
3. The location and magnitude of the mean activity maximum associated with the core population at $\lambda_\odot = 139°.96 \pm 0°.05$ and with $S_{6.5\ \max} = 96 \pm 16 \times 10^9$ km^3.
4. The change in particle composition across the stream, particularly in the region near the maxima in r at $\lambda_\odot = 139°.55 \pm 0°.07$ and $\lambda_\odot = 139°.88 \pm 0°.06$.
5. The apparent similarity between the meteoroid populations associated with the outburst and the core population.
6. The broad shoulder in flux after the core maximum.
7. The differing slopes in the branches of the outburst profile and the asymmetry in these profiles.
8. The origins of the background, outburst, and core populations.

Other characteristics which are not conclusively discerned in these data, such as the possible presence of a sub-maximum near $\lambda_\odot = 140°.2–140°.3$ or at $\lambda_\odot = 140°.5$ and the existence of ephemeral sub-maxima at various locations after the core maximum in different years, need further observational confirmation. The use of visual or photographic data from only one or a few locations may lead to erroneous determinations for the peak flux and activity profile for a meteor stream, particularly in cases where only small quantities of such data are available.

In conclusion, the Perseid meteoroid stream is highly dynamic and rich in structure. The complexities of the Perseids can be understood only in the context of a complete numerical model of the stream and must explain features detected through observations such as those found here.

ACKNOWLEDGMENTS

The authors are deeply indebted to all observers who contributed their observations to this study. Without their dedication this work would not have been possible. P.B. thanks the Natural Sciences and Engineering Research Council for funding support. Helpful reviews by J. Jones, K. Yau, R. Koschack, and an anonymous referee are gratefully acknowledged.

REFERENCES

Ahnert–Rohlfs, E. 1952. On the structure and the origin of the Perseid meteoroid stream. *Veröffentlichungen der Sternwarte Sonneberg* **2,** 5–38.

Andreev, G. V., L. N. Rubtsov, and N. V. Tarasova 1987. On the spatial structure of the Perseids meteor stream. In *First GLOBMET Symposium* (R. G. Roper, Ed.), p. 339. ICSU-SCOSTEP, Urbana, Illinois.

Bellot Rubio, L. R. 1995. Effects of the dependence of meteor brightness on the entry angle. *Astron. Astrophys.* **301,** 602–608.

Harris, N. W., K. C. C. Yau, and D. W. Hughes 1995. The true extent of the nodal distribution of the Perseid meteoroid stream. *Mon. Not. R. Astron. Soc.* **273,** 999–1015.

Hasegawa, I. 1993. Historical records of meteor showers. In *Meteoroids and Their Parent Bodies*, J. Štohl and I. P. Williams, (Eds.), p. 209. Astronomical Inst., Slovak Acad. Sci., Bratislava.

Jones, J., and P. Brown 1993. Sporadic meteor radiant distributions: Orbital survey results. *Mon. Not. R. Astron. Soc.* **265,** 524–532.

Jones, J., and P. Brown 1996. Modelling the orbital evolution of the Perseid meteoroids. In *Physics, Chemistry and Dynamics of Interplanetary Dust* (B. Å. S Gustafson and M. S. Hanner, Eds.), p. 105. Astronomical Society of the Pacific.

Kaiser, T. R., L. M. G. Poole, and A. R. Webster 1966. Radio-echo observations of the major night-time streams. I. Perseids. *Mon. Not. R. Astron. Soc.* **132,** 224–237.

Koschack, R. 1994. Single body theory and zenith correction factor. In *Proceedings of the International Meteor Conference Belogradchik, Bulgaria, 22–25 Sept. 1994.* (A. Knöfel and P. Roggemans, Eds.), pp. 31–43. IMO, Mechelen.

Koschack, R. 1995. Analyses and calculations. In *Handbook for Visual Meteor Observers* (J. Rendtel, R. Arlt, and A. McBeath, Eds.), pp. 280–289. IMO, Potsdam.

Koschack, R., R. Arlt, and J. Rendtel 1993. Global analysis of the 1991 and 1992 Perseids. *WGN J. IMO* **21**(4), 152–168.

Koschack, R., and R. L. Hawkes 1995. Observing instructions for major meteor showers. In *Handbook for Visual Meteor Observers.* (J. Rendtel, R. Arlt, and A. McBeath, Eds.), pp. 42–74. IMO, Potsdam.

Koschack, R., and J. Rendtel 1988. Number density in meteor streams. *WGN J. IMO* **16,** 149–157.

Koschack, R., and J. Rendtel 1990a. Determination of spatial number density and mass index from visual meteor observations. *WGN J. IMO* **18,** 44–59.

Koschack, R., and J. Rendtel 1990b. Determination of spatial number density and mass index from visual meteor observations (II). *WGN J. IMO* **18,** 119–141.

Koschack, R., and P. Roggemans 1991. The 1989 Perseid meteor stream. *WGN J. IMO* **19,** 87–99.

Kresáková, M. 1966. The magnitude distribution of meteors in meteor streams. *Contr. Skalnaté. Pleso* **3,** 75–109.

Kronk, G. W. 1988. *Meteor Showers: A Descriptive Catalog.* Enslow, New Jersey.

Lindblad, B. A. 1986. Structure and activity of the Perseid meteor stream from visual observations 1953–1981. In *Asteroids, Comets, Meteors II,* (C.-I. Lagerkvist, B. A. Lindblad, H. Lundstedt, and H. Rickman, Eds.), p. 531. Reprocentralen, Uppsala.

Lindblad, B. A., and V. Porubčan 1994. The activity and orbit of the Perseid meteor stream, *Planet. Space Sci.* **42,** 117–123.

Lindblad, B. A., and M. Šimek 1986. The activity curve of the Perseid meteor stream from Onsala radar observations 1953–78. In *Asteroids, Comets, Meteors II* (C.-I. Lagerkvist, B. A. Lindblad, H. Lundstedt, and H. Rickman, Eds.), p. 537. Reprocentralen, Uppsala.

Lovell, A. C. B. 1954, *Meteor Astronomy.* Oxford Univ. Press, London.

Marsden, B. G. 1973. The next return of the comet of the Perseid meteors. *Astron. J.* **78,** 654–662.

Marsden, B. G., G. V. Williams, G. W. Kronk, and W. G. Waddington 1993. Update on Comet Swift–Tuttle. *Icarus,* **105,** 420–426.

Mason, J. W., and I. Sharp 1981. The Perseid meteor stream in 1980. *JBAA* **91,** 368–390.

McKinley, D. W. R. 1961. *Meteor Science and Engineering.* McGraw–Hill, Toronto.

Öpik, E. J. 1922. Instructions for statistical observation of shooting stars (double count method). *Publ. Tartu Observ.* **25,** 48–56.

Pin–Xin, X. 1992. The 1992 Perseid outburst in China. *WGN J. IMO* **20,** 198.

Rendtel, J., P. Brown, and S. Molau 1996. The 1995 outburst and possible origin of the α-Monocerotid meteoroid stream. *Mon. Not. R. Astron. Soc.* **279,** L31–L36.

Roggemans, P. 1989. The Perseid meteor stream in 1988: A double maximum! *WGN J. IMO* **17,** 127–137.

Schiaparelli, G. V. 1867. Sur les Étoiles Filantes, et spécialement sur l'identification der Orbites des Essaims d'Août et de Novembre avec celles des Comètes de 1862 et de 1866. *Comptes Rendus* **64,** 598–599.

Šimek, M., and B. A. McIntosh 1986. Perseid meteor stream: Mean flux curve from radar observations, *BAC* **37,** 146–155.

Šimek, M. 1987. Perseid meteor stream mean profile from radar observations in Czechoslovakia. *BAC* **38,** 1–6.

Šimek, M., and P. Pecina 1996. Activity of the new filament in the Perseid meteor stream. In *Physics, Chemistry and Dynamics of Interplanetary Dust* (B. Å. S Gustafson and M. S. Hanner, Eds.), p. 109. Astronomical Society of the Pacific.

Verniani, F. 1973, An analysis of the physical parameters of 5759 faint radio meteors. *J. Geophys. Res.* **78,** 8429–8462.

Watanabe, J.–I., T. Nakamura, M. Tsutsumi, and T. Tsuda 1992. Radar observations of the strong activity of a Perseid meteor shower in 1991. *PASJ* **44,** 677–685.

Williams, I. P., and Z. Wu 1994. The current Perseid meteor shower. *Mon. Not. R. Astron. Soc.* **269,** 524–528.

Wu, Z., and I. P. Williams 1993. The Perseid meteor shower at the current time. *Mon. Not. R. Astron. Soc.* **264,** 980–990.

Wu, Z., and I. P. Williams 1995. Gaps in the semimajor axes of the Perseid meteors. *Mon. Not. R. Astron. Soc.* **276,** 1017–1023.

Yau, K., D. Yeomans, and P. R. Weissman 1994. The past and future motion of Comet P/Swift–Tuttle. *Mon. Not. R. Astron. Soc.* **266,** 303–316.

Zvolánková, V. 1983. Dependence of the observed rate of meteors on the zenith distance of the radiant. *BAC* **34,** 372–375.

Zvolánková, V. 1984. Changes in the activity of the Perseid meteor shower 1944–1953. *Contr. Obs. Skalnaté Pleso* **12,** 45–75.